NUMERICAL SIMULATION OF INTERACTION BETWEEN INCOMPRESSIBLE FLOW AND AN ELASTIC WALL[*]

MARTIN HADRAVA[†], MILOSLAV FEISTAUER[‡], AND PETR SVÁČEK[§]

Abstract. The present paper is devoted to the numerical solution to flow in time-dependent domains with elastic walls. This problem has several applications in engineering and medicine. The flow is described by the system of Navier-Stokes equations supplemented with suitable initial and boundary conditions. A part of the boundary of the region occupied by the fluid is represented by an elastic wall, whose deformation is driven by a hyperbolic partial differential equation with initial and boundary conditions. Its right-hand side represents the force by which the fluid flow acts on the elastic wall. A numerical method for solving this coupled problem is elaborated, based on the finite element method and the arbitrary Lagrangian-Eulerian (ALE) formulation of the equations describing the flow. The formulation and analysis of the problem together with discretization, algorithmization and programming of modules, which were added to an existing software package, is presented. The developed method is applied to solving test problems.

Key words. fluid-structure interaction, Navier-Stokes equations, arbitrary Lagrangian-Eulerian method, finite element method, string equation

AMS subject classifications. 35Q30, 74F10, 76D05

1. Introduction. Interaction of flow with an elastic structure plays an important role in contemporary research and industry. Among the most significant areas of application one can mention aerospace engineering, civil engineering, car industry or medicine. The presented work is concerned with medical applications by modeling fluid flow in a channel with elastic walls, which may represent the walls of human vocal folds or vessels. This subject is in the center of attention particularly with respect to modelling and simulation of cardio-vascular systems. Various aspects are treated, e.g., in [4], [6] and [7], where a general framework of the fluid-structure coupling and some iterative procedures can be found.

In this article we describe a numerical method developed for the simulation of the vibrations of an elastic wall induced by viscous incompressible flow. The fluid flow is described by the system of incompressible Navier-Stokes equations supplemented with the continuity equation. Movement of the elastic wall of the two-dimensional channel occupied by the fluid is described by the string hyperbolic partial differential equation. The time dependence of the domain occupied by the fluid is taken into account by the arbitrary Lagrangian-Eulerian (ALE) method. Both the fluid and the structure problem are then semi-discretized in time by the backward-difference formula of second order and the resulting equations are discretized in space using a conforming finite element method (FEM). The applicability of the developed method

[†]Department of Numerical Mathematics, Faculty of Mathematics and Physics, Charles University in Prague, Sokolovská 83, 186 75 Praha 8, Czech Republic (`martin@hadrava.eu`).

[‡]Department of Numerical Mathematics, Faculty of Mathematics and Physics, Charles University in Prague, Sokolovská 83, 186 75 Praha 8, Czech Republic (`feist@karlin.mff.cuni.cz`).

[§]Department of Technical Mathematics, Faculty of Mechanical Engineering, Czech Technical University in Prague, Karlovo nám. 13, 121 35 Praha 2, Czech Republic (`Petr.Svacek@fs.cvut.cz`).
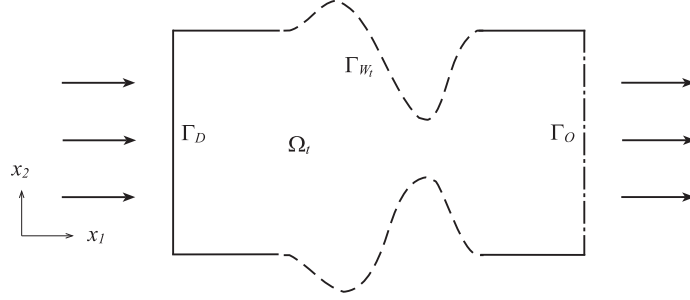
is demonstrated by numerical experiments.

FIG. 1.1. *Plane channel with elastic walls.*

2. Governing equations.

2.1. Structure of the domain occupied by the fluid. We deal with incompressible flow in a bounded plane domain $\Omega_t \subset \mathbb{R}^2$ depending on time $t \in [0, T)$, $T > 0$. Figure 1.1 shows an example of such domain with two elastic walls. For the sake of simplicity, only a single elastic wall will be considered. The boundary $\partial \Omega_t$ of the domain occupied by the fluid is split according to prescribed boundary conditions into three disjoint parts, $\partial \Omega_t = \Gamma_D \cup \Gamma_O \cup \Gamma_{W_t}$. The part of the boundary Γ_D represents the inlet and fixed impermeable parts of the walls. Γ_O represents the outlet of the channel. Finally, Γ_{W_t} represents the elastic wall and is time-dependent.

2.2. The Navier-Stokes equations. We use the notation

$$\mathcal{M} = \{(\boldsymbol{x}, t); \boldsymbol{x} \in \Omega_t, t \in (0, T)\} \qquad \text{and} \qquad \tilde{\Gamma} = \{(\boldsymbol{x}, t); \boldsymbol{x} \in \Gamma_{W_t}, t \in (0, T)\}.$$

The fluid flow is described by the following system of equations and boundary and initial conditions:

$$\frac{\partial \boldsymbol{u}}{\partial t} + (\boldsymbol{u} \cdot \nabla) \boldsymbol{u} + \nabla p - \nu \Delta \boldsymbol{u} = 0 \qquad \text{in } \mathcal{M}, \tag{2.1}$$

$$\text{div} \boldsymbol{u} = 0 \qquad \text{in } \mathcal{M}, \tag{2.2}$$

$$\boldsymbol{u} = \boldsymbol{u}_D \qquad \text{on } \Gamma_D \times (0, T), \tag{2.3}$$

$$-p\boldsymbol{n} + \nu \frac{\partial \boldsymbol{u}}{\partial \boldsymbol{n}} = -p_{ref} \boldsymbol{n} \quad \text{on } \Gamma_O \times (0, T), \tag{2.4}$$

$$\boldsymbol{u} = \boldsymbol{w} \qquad \text{on } \tilde{\Gamma}, \tag{2.5}$$

$$\boldsymbol{u} = \boldsymbol{u}_0 \qquad \text{in } \Omega_0, \tag{2.6}$$

where the velocity of viscous incompressible flow is denoted by $\boldsymbol{u}$ and the kinematic pressure of the fluid is denoted by p. We consider the incompressible Navier-Stokes equations in the form (2.1) supplemented with the continuity equation (2.2). Here the constant $\nu > 0$ denotes the kinematic viscosity of the fluid. On Γ_D the Dirichlet boundary condition (2.3) is prescribed, where $\boldsymbol{u}_D$ is a given function. On Γ_O the so-called "do-nothing" boundary condition (2.4) is prescribed, where $\boldsymbol{n}$ denotes the unit outer normal to Ω_t and p_{ref} denotes a reference pressure prescribed on the outlet. On the moving wall Γ_{W_t} the Dirichlet boundary condition (2.5) is prescribed, where $\boldsymbol{w}$ denotes the velocity of the elastic wall deformation. A rigorous definition of the quantity $\boldsymbol{w}$ is given below (cf. equation (2.10)). The system of equations is finally completed by the initial condition (2.6), where $\boldsymbol{u}_0$ is a given function.

2.3. String equation. Deformation of the elastic wall is described by the following initial boundary-value problem:

$$\frac{\partial^2 \eta}{\partial t^2} - a\frac{\partial^2 \eta}{\partial x_1^2} + b\eta - c\frac{\partial^3 \eta}{\partial t \partial x_1^2} + d\frac{\partial \eta}{\partial t} = H \quad \text{in } Q, \tag{2.7}$$

$$\eta = \eta_0, \frac{\partial \eta}{\partial t} = \eta_1 \quad \text{in } (0, L) \text{ at } t = 0, \tag{2.8}$$

$$\eta = 0, \frac{\partial \eta}{\partial t} = 0 \quad \text{in } (0, T) \text{ at } x_1 = 0 \text{ and } x_1 = L, \tag{2.9}$$

where the string hyperbolic partial differential equation (2.7) is valid in the domain $Q = (0, L) \times (0, T)$, $L > 0$. Here the function η denotes the deformation of the wall in the direction of the x_2-axis, a, b, c, d are positive constants characterizing properties of the wall and the function H represents the x_2-component of the force by which the fluid acts on the elastic wall. Equation (2.7) is supplemented with the initial conditions (2.8), where η_0 and η_1 are given functions, and the homogeneous boundary conditions (2.9). The derivation of the presented model can be found in [10]. We assume that the elastic wall Γ_{W_t} can be parametrized by a smooth function $\sigma = \sigma_0 + \eta$, $\sigma : Q \to \mathbb{R}$, where σ_0 parametrizes Γ_{W_t} at $t = 0$ and η represents the deformation of the elastic wall. The right-hand side H of equation (2.7) is defined by the relation

$$H = \frac{1}{\rho_w h_w} \sum_{j=1}^{2} n_j \tau_{j2},$$

where $\boldsymbol{n} = (n_1, n_2)$ is the unit outer normal to Ω_t, $\rho_w > 0$ is the constant density of the elastic wall, $h_w > 0$ is its constant thickness and $\tau = (\tau_{ij})_{i,j=1}^2$ is the fluid stress tensor (cf. [3]). Finally, the velocity of the elastic wall deformation is defined by

$$\boldsymbol{w} = \left(0, \frac{\partial \eta}{\partial t}\right). \tag{2.10}$$

From the presented equations it follows that the fluid flow problem depends on the solution to the string deformation problem through the boundary condition (2.5) and the string deformation problem depends on the solution to the fluid flow problem through the right-hand side H of equation (2.7).
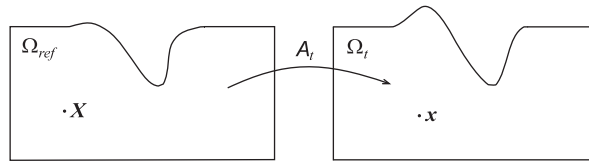

FIG. 3.1. *ALE mapping $\mathcal{A}_t$.*

3. ALE formulation. In order to simulate flow in a time-dependent domain the ALE method is employed. Let us denote the *reference configuration* by $\Omega_{ref} = \Omega_0$, i.e. the reference configuration is the computational domain Ω_t at time $t = 0$. A smooth, one-to-one mapping of $\overline{\Omega}_{ref}$ onto $\overline{\Omega}_t$ at time t (the so-called *current configuration*) is denoted by $\mathcal{A}_t$ (cf. [8], see Fig. 3.1), i.e.

$$\mathcal{A}_t : \overline{\Omega}_{ref} \to \overline{\Omega}_t, \ \mathcal{A}_t : \boldsymbol{X} \mapsto \boldsymbol{x} = \mathcal{A}_t(\boldsymbol{X}).$$

The ALE mapping $\mathcal{A}_t$ serves as a basis for the definition of the *domain velocity*

$$\tilde{\boldsymbol{w}}(\boldsymbol{X}, t) = \frac{\partial}{\partial t}\mathcal{A}_t(\boldsymbol{X}), \quad \boldsymbol{X} \in \Omega_{ref}, \, t \in (0, T),$$

$$\boldsymbol{w}(\boldsymbol{x}, t) = \tilde{\boldsymbol{w}}(\boldsymbol{X}, t), \quad \boldsymbol{X} = \mathcal{A}_t^{-1}(\boldsymbol{x}), \, \boldsymbol{x} \in \Omega_t, \, t \in (0, T).$$

We use the symbol $\boldsymbol{w}$ to denote the ALE velocity since its restriction to Γ_{W_t} is the velocity of the elastic wall (see equation (2.10)). The *ALE derivative* of a function $f = f(\boldsymbol{x}, t)$ is defined as

$$\frac{D^{\mathcal{A}}f}{Dt}(\boldsymbol{x}, t) = \frac{\partial \tilde{f}}{\partial t}(\boldsymbol{X}, t),$$

where

$$\tilde{f}(\boldsymbol{X}, t) = f(\mathcal{A}_t(\boldsymbol{X}), t), \, \boldsymbol{X} = \mathcal{A}_t^{-1}(\boldsymbol{x}) \in \Omega_{ref}, \, \boldsymbol{x} \in \Omega_t, \, t \in (0, T).$$

From the chain rule it follows that $\dfrac{D^{\mathcal{A}}f}{Dt} = \dfrac{\partial f}{\partial t} + (\boldsymbol{w} \cdot \nabla)f$, which yields the ALE form of the Navier-Stokes equations

$$\frac{D^{\mathcal{A}}\boldsymbol{u}}{Dt} + ((\boldsymbol{u} - \boldsymbol{w}) \cdot \nabla)\boldsymbol{u} + \nabla p - \nu\Delta\boldsymbol{u} = 0. \tag{3.1}$$

4. Discretization of the Navier-Stokes equations.

4.1. Time discretization. For the time semi-discretization of equations (2.2) and (3.1) the second-order backward difference formula is applied. We introduce a uniform partition $0 = t_0 < \cdots < t_N = T$, $t_k = k\tau$, of the time interval $[0, T]$ with a constant time step $\tau > 0$. The exact solution $(\boldsymbol{u}, p)$ to the Navier-Stokes system at time t_n is approximated by the couple $(\boldsymbol{u}^n, p^n)$. The time derivative of $\boldsymbol{u}$ is discretized as

$$\frac{D^{\mathcal{A}}\boldsymbol{u}}{Dt}(\boldsymbol{x}, t_{n+1}) \approx \frac{3\boldsymbol{u}^{n+1}(\boldsymbol{x}) - 4\hat{\boldsymbol{u}}^n(\boldsymbol{x}) + \hat{\boldsymbol{u}}^{n-1}(\boldsymbol{x})}{2\tau}, \, \boldsymbol{x} \in \Omega_{t_{n+1}}, \tag{4.1}$$

where $\hat{\boldsymbol{u}}^j = \boldsymbol{u}^j \circ \mathcal{A}_{t_j} \circ \mathcal{A}_{t_{n+1}}^{-1}$, $j = n-1, n$. Replacing the ALE derivative of the fluid velocity $\boldsymbol{u}$ with the term on the right-hand side of approximation (4.1) yields a system of stationary PDEs

$$\frac{3\boldsymbol{u}^{n+1} - 4\hat{\boldsymbol{u}}^n + \hat{\boldsymbol{u}}^{n-1}}{2\tau} + \left((\boldsymbol{u}^{n+1} - \boldsymbol{w}^{n+1}) \cdot \nabla\right)\boldsymbol{u}^{n+1} + \nabla p^{n+1} - \nu\Delta\boldsymbol{u}^{n+1} = 0, \tag{4.2}$$

$$\text{div}\,\boldsymbol{u}^{n+1} = 0$$

for unknown functions $\boldsymbol{u}^{n+1}$, p^{n+1}. By $\boldsymbol{w}^{n+1}$ we denote the approximation of the function $\boldsymbol{w}(\cdot, t_{n+1})$.

4.2. Space discretization.

4.2.1. Weak formulation. Space discretization is carried out using a conforming finite element method (FEM). In this section we simply write $\boldsymbol{u}$, p, Ω and $\boldsymbol{w}$ instead of $\boldsymbol{u}^{n+1}$, p^{n+1}, $\Omega_{t_{n+1}}$ and $\boldsymbol{w}^{n+1}$. At first, equations (4.2) are multiplied by test functions $\boldsymbol{v} \in \mathcal{X}$ and $q \in \mathcal{Q}$ respectively, where

$$\mathcal{X} = \left\{\boldsymbol{v} \in (H^1(\Omega))^2; \boldsymbol{v}|_{\Gamma_D \cup \Gamma_{W_t}} = 0\right\}$$

and $\mathcal{Q} = L^2(\Omega)$, $H^1(\Omega)$ is the Sobolev space of $L^2(\Omega)$ functions with the first-order derivatives in $L^2(\Omega)$ and $L^2(\Omega)$ is the Lebesgue space of square-integrable functions on Ω. We further write $\mathcal{W} = (H^1(\Omega))^2$. Integrating the resulting equations over Ω, summing them and using Green's theorem for the terms containing $\Delta \boldsymbol{u}$ and ∇p, the weak formulation of equations (4.2) is obtained: Find $U = (\boldsymbol{u}, p) \in \mathcal{W} \times \mathcal{Q}$ such that

$$a(U, U, V) = f(V) \quad \text{for all} \quad V = (\boldsymbol{v}, q) \in \mathcal{X} \times \mathcal{Q}. \tag{4.3}$$

We assume that the function $\boldsymbol{u}$ satisfies the boundary conditions (2.3) and (2.5) at time t_{n+1}. The terms $a(U, U, V)$ and $f(V)$ are defined by

$$a(U^*, U, V) = \frac{3}{2\tau}(\boldsymbol{u}, \boldsymbol{v})_\Omega + (((\boldsymbol{u}^* - \boldsymbol{w}) \cdot \nabla)\boldsymbol{u}, \boldsymbol{v})_\Omega - (p, \text{div}\boldsymbol{v})_\Omega + \nu((\boldsymbol{u}, \boldsymbol{v}))_\Omega$$
$$+ (\text{div}\boldsymbol{u}, q)_\Omega,$$

$$f(V) = \frac{1}{2\tau}(4\hat{\boldsymbol{u}}^n - \hat{\boldsymbol{u}}^{n-1}, \boldsymbol{v})_\Omega - \int_{\Gamma_O} p_{ref}\boldsymbol{v} \cdot \boldsymbol{n} \, \text{d}S,$$

where $U^* = (\boldsymbol{u}^*, p) \in \mathcal{W} \times \mathcal{Q}$, $U = (\boldsymbol{u}, p) \in \mathcal{W} \times \mathcal{Q}$, $V = (\boldsymbol{v}, q) \in \mathcal{X} \times \mathcal{Q}$ and $(f, g)_\Omega = \int_\Omega fg \, \text{d}\boldsymbol{x}$ denotes the scalar product in $L^2(\Omega)$ or in $(L^2(\Omega))^2$ and $((\boldsymbol{u}, \boldsymbol{v}))_\Omega$ denotes the bilinear form

$$((\boldsymbol{u}, \boldsymbol{v}))_\Omega = \int_\Omega \nabla \boldsymbol{u} \cdot \nabla \boldsymbol{v} \, \text{d}\boldsymbol{x} = \sum_{i,j=1}^{2} \int_\Omega \frac{\partial u_i}{\partial x_j} \frac{\partial v_i}{\partial x_j} \, \text{d}\boldsymbol{x},$$

where $\boldsymbol{u} = (u_1, u_2)$ and $\boldsymbol{v} = (v_1, v_2)$. The couple $(\boldsymbol{u}, p)$ represents the approximate solution to the fluid flow problem at the time level t_{n+1}.

4.2.2. Finite element method. We approximate the spaces $\mathcal{W}$, $\mathcal{X}$ and $\mathcal{Q}$ from the weak formulation (4.3) by finite dimensional subspaces $\mathcal{W}_h$, $\mathcal{X}_h$ and $\mathcal{Q}_h$, $h \in (0, h_0)$, $h_0 > 0$, where $\mathcal{X}_h = \{\boldsymbol{v}_h \in \mathcal{W}_h; \boldsymbol{v}_h|_{\Gamma_D \cup \Gamma_{W_t}} = 0\}$. We define the discrete problem to find $U_h = (\boldsymbol{u}_h, p_h) \in \mathcal{W}_h \times \mathcal{Q}_h$ such that the equation
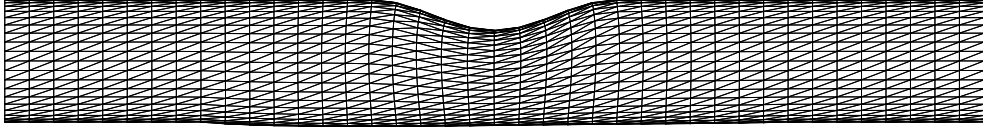
$$a(U_h, U_h, V_h) = f(V_h)$$

is satisfied for all $V_h = (\boldsymbol{v}_h, q_h) \in \mathcal{X}_h \times \mathcal{Q}_h$ and $\boldsymbol{u}_h$ approximately satisfies prescribed boundary conditions. Because of the stability of the method, finite-dimensional spaces $\mathcal{X}_h, \mathcal{Q}_h$ that satisfy the Babuška-Brezzi condition (cf. [1]) are chosen. This means that there exists a positive constant $c > 0$ such that

$$\sup_{0 \neq \boldsymbol{v} \in \mathcal{X}_h} \frac{(p, \text{div}\boldsymbol{v})_\Omega}{|\boldsymbol{v}|} \geq c||p||$$

holds for all $p \in \mathcal{Q}_h, h \in (0, h_0)$. Here $|\cdot|$ denotes the $(H^1(\Omega))^2$ semi-norm defined by $|\boldsymbol{v}| = ((\boldsymbol{v}, \boldsymbol{v}))_\Omega^{1/2}$ and $||\cdot||$ denotes the $L^2(\Omega)$ norm defined by $||p|| = (p, p)_\Omega^{1/2}$.

In practical realization the domain Ω is assumed to be a polygonal approximation of the region occupied by the fluid at time t_{n+1}. $\mathcal{T}_h$ denotes the triangulation of the domain Ω with standard properties from the FEM. Figure 4.1 shows an example of a triangular mesh of the domain Ω. We employ the Taylor-Hood P^2/P^1-elements (cf. [1]), where the pressure p is approximated by a continuous function p_h, which is linear on each triangle $K \in \mathcal{T}_h$, and the fluid velocity $\boldsymbol{u}$ is approximated by a continuous function $\boldsymbol{u}_h$, which is quadratic in each component on each triangle $K \in \mathcal{T}_h$. The couple $(\mathcal{X}_h, \mathcal{Q}_h)$ defined in this way satisfies the Babuška-Brezzi condition (cf. [1]).

FIG. 4.1. *Triangular mesh $\mathcal{T}_h$ of the domain Ω.*

4.2.3. Linearization. The resulting strongly non-linear problem is linearized by the application of the Oseen iterative process (cf. [3], page 599). Each Oseen iteration is equivalent to the system of linear algebraic equations with a non-symmetric matrix

$$\left(\begin{array}{cc} \mathbf{A} & \mathbf{B} + \mathbf{C} \\ \mathbf{B}^T & 0 \end{array} \right) \left(\begin{array}{c} \boldsymbol{U} \\ \boldsymbol{P} \end{array} \right) = \left(\begin{array}{c} \boldsymbol{F} \\ \boldsymbol{G} \end{array} \right), \tag{4.4}$$

where the vector $\boldsymbol{U}$ denotes the coefficients of an approximation of the discrete fluid velocity with respect to the chosen basis of the space $\mathcal{W}_h$ and the vector $\boldsymbol{P}$ denotes the coefficients of an approximation of the discrete pressure with respect to the chosen basis of the space $\mathcal{Q}_h$.

The solution to the system (4.4) is realized by the direct solver UMFPACK (cf. [2]), which works sufficiently fast for systems with up to 10^5 equations.
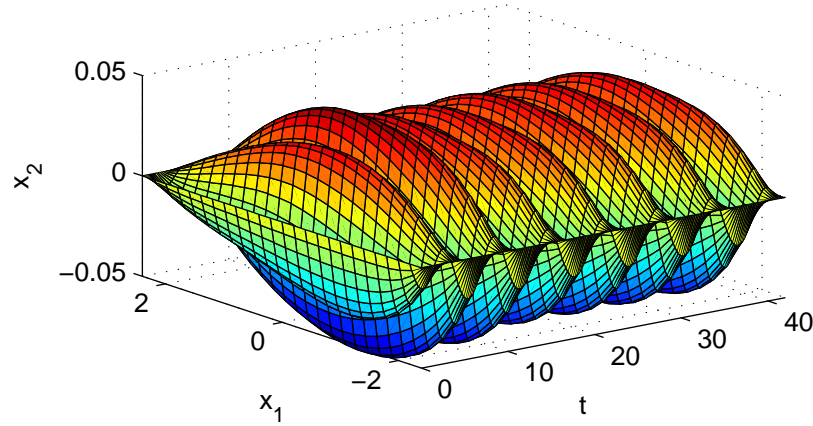
5. Discretization of the string equation. In this section we denote $x = x_1$. The string equation (2.7), which is of the second order in time, is transformed to the couple of the first-order differential equations

$$\frac{\partial \xi}{\partial t} - a \frac{\partial^2 \eta}{\partial x^2} + b\eta - c \frac{\partial^2 \xi}{\partial x^2} + d\xi = H, \quad \frac{\partial \eta}{\partial t} = \xi, \tag{5.1}$$

where ξ denotes the velocity of the elastic wall deformation. Equations (5.1) are semi-discretized in time with the aid of the backward-difference formula of second order of accuracy, similarly as in the time semi-discretization of the Navier-Stokes equations. The resulting equations are then discretized in space employing the conforming finite element method with linear elements. The resulting stiffness matrix $\mathbf{S}$ is block-banded, indefinite and non-symmetric. Since the number of degrees of freedom in this case is low, the solution to the wall deformation problem can be obtained with the aid of a direct solver.
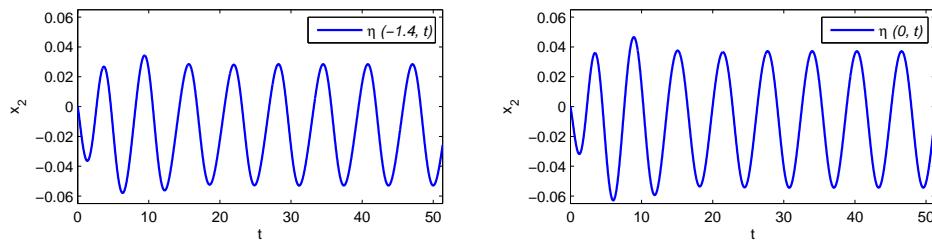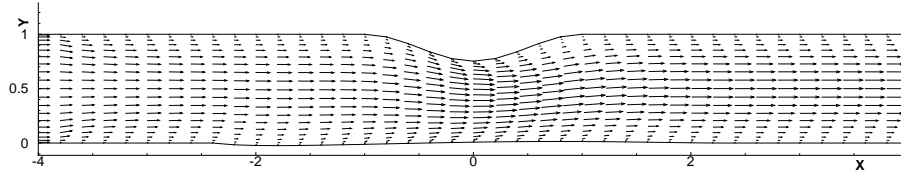
6. Numerical experiments.

6.1. Complete discrete problem. The following numerical experiments were obtained using a modified software package FEMFLUID (cf. [9]). Numerical methods for solving the flow problem and the wall deformation problem separately were presented in the preceding sections. Prior to presenting results of the main test problem we introduce a method to deal with the interaction problem. A technique based on the so-called *predictor-corrector* method is employed. At the time level t_n the right-hand side H of equation (2.7) is computed. The obtained result is then used to compute an approximation to the wall deformation η at time t_{n+1} and subsequently an approximation of the domain occupied by the fluid at time t_{n+1} is obtained. Now we solve numerically the flow problem at the time level t_{n+1} and use the obtained results to update the approximation of the right-hand side H of equation (2.7). If H changes by more than a prescribed tolerance, we repeat the whole process to obtain a better

Fig. 6.1. *Evolution of the deformation of the elastic wall in time.*

approximation of the wall deformation η and subsequently a better approximation of the flow problem solution.

6.2. Test problem. In the presented numerical experiment it is assumed that the upper wall movement is prescribed by a sufficiently smooth time-periodic function. The upper wall movement induces movement of the lower elastic wall. The main parameters of the numerical experiment are given as follows: $\tau = 0.01$, $T = 40$, $\nu = 0.01$. The corresponding Reynolds number Re is defined by the relation $Re = UL/\nu$ and therefore equals 100. Here U denotes the characteristic velocity (in our case the prescribed flow velocity at the channel inlet) and L denotes the characteristic length (in our case the width of the channel at the inlet). Figure 6.1 shows the evolution of the deformation of the elastic wall in time. Figure 6.2 shows the graph of the movement of two points of the elastic wall with the first coordinate given by $x_1 = -1.4$ and $x_1 = 0$. Finally, Figure 6.3 shows the velocity field at time $t = 7.9$. The triangular mesh used in this example has 1600 elements. The number of degrees of freedom in the fluid flow problem is 7503, while the number of degrees of freedom in the elastic wall deformation problem is 46. The computational time on a standard dual-core laptop was approximately 12 hours. Details about the numerical experiment can be found in [5].

Fig. 6.2. *Graph of the movement of a point with the first coordinate $x_1 = -1.4$ (left) and $x_1 = 0$ (right).*

FIG. 6.3. *Velocity field $\boldsymbol{u}$ at time $t = 7.9$. Here $\mathbf{X} = x_1$ and $\mathbf{Y} = x_2$.*

6.3. Estimated rate of convergence. In the case of the presented numerical example the estimated order of convergence (EOC) of the approximate solution to the elastic wall deformation was numerically computed. Triangular meshes of the computation domain with spatial steps $h = 1$, 0.5, 0.25 and 0.125 were constructed. Then the approximate solutions to our problem with time steps $\tau = 0.16$, 0.08, 0.04, 0.02 and 0.01 for all available spatial meshes were computed. From the numerical results we could then deduce whether the estimate of the error, measured in the L^2-norm, is dominated by the term dependent on the spatial step h or the term dependent on the time step τ. Since the exact solution is unknown, we used the approximate solution obtained with a very fine triangular mesh ($h = 0.00625$) and a very small time step ($\tau = 0.005$). Our aim was to compare the so-called weak coupling (i.e. computing the predictor only) with the so-called strong coupling (in our case, computing the predictor and subsequently 3-times the corrector) of the fluid-structure problem.

Figure 6.4 shows a comparison of the elastic wall deformation using different time steps at several time instants, employing both the predictor and the predictor-corrector technique. Table 6.2 shows the EOC of the approximate solution of the elastic wall deformation to the exact solution (assuming that it exists) in time, while Table 6.1 shows the EOC in space. Finally, Table 6.3 shows the average EOC both in time and space.

$h = 0.125$	Time value t			$h = 0.125$	Time value t		
τ	5.76	7.36	8.64	τ	5.76	7.36	8.64
0.16 / 0.08	0.705	0.237	0.526	0.16 / 0.08	0.973	1.752	2.093
0.08 / 0.04	1.078	0.985	1.016	0.08 / 0.04	1.016	1.519	0.761
0.04 / 0.02	1.133	1.782	1.193	0.04 / 0.02	1.152	1.383	0.714
0.02 / 0.01	0.972	0.218	0.853	0.02 / 0.01	1.677	1.557	1.274

TABLE 6.1

Estimated order of convergence in time using the predictor technique (left) and the predictor-corrector technique (right).

$\tau = 0.005$	Time value t			$\tau = 0.005$	Time value t		
h	5.76	7.36	8.64	h	5.76	7.36	8.64
1 / 0.5	1.324	0.855	0.298	1 / 0.5	1.445	1.236	0.347
0.5 / 0.25	1.796	1.865	3.215	0.5 / 0.25	2.423	2.389	4.243

TABLE 6.2

Estimated order of convergence in space using the predictor technique (left) and the predictor-corrector technique (right).
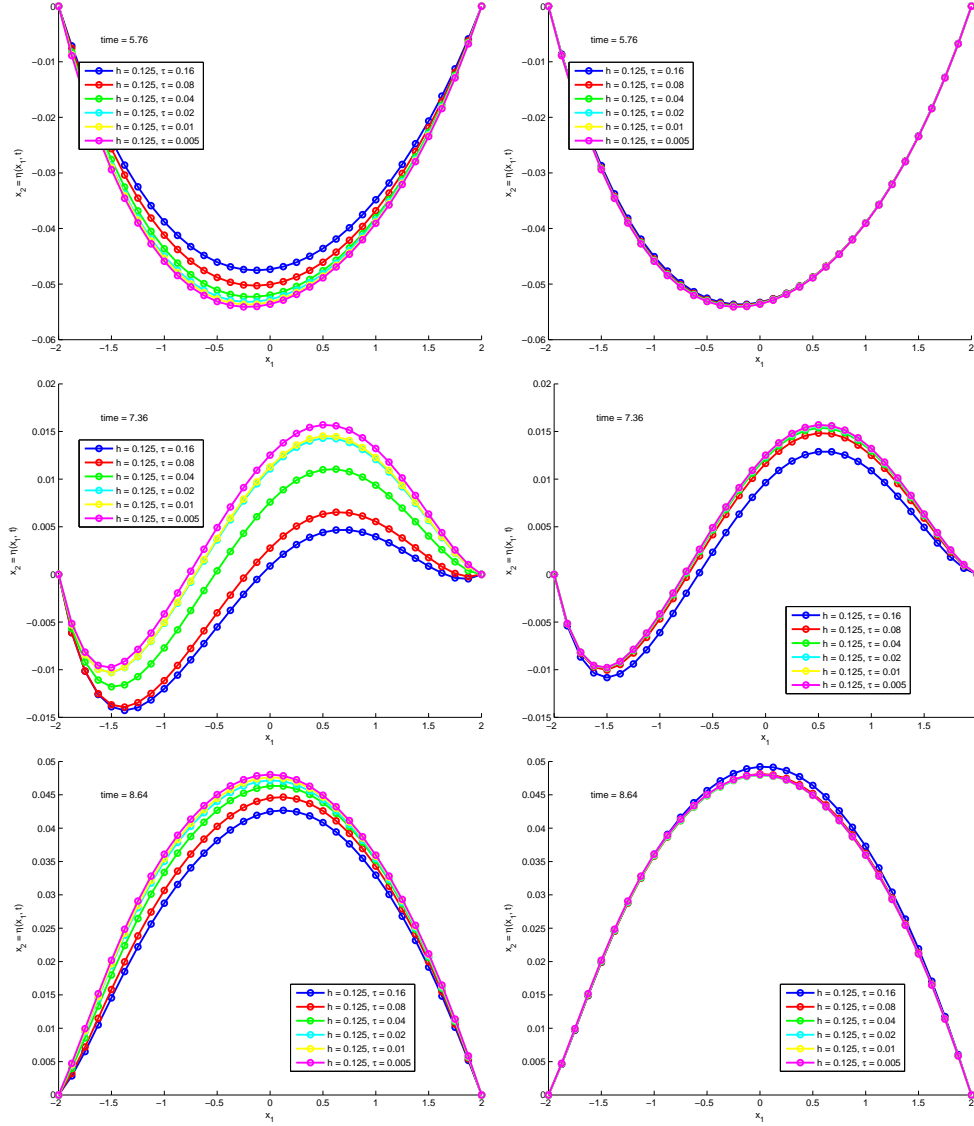
FIG. 6.4. *Comparison of the elastic wall deformation using different time steps at time $t = 5.76$ (top), $t = 7.36$ (middle) and $t = 8.64$ (bottom) using the predictor technique (left) and predictor-corrector technique (right).*

From the tables it can be seen that the EOC differs largely using different couples of triangular meshes or time steps and observing the estimated errors at different time instants. Nevertheless, the figures clearly indicate that choosing the predictor-corrector technique allows us to set a larger time step while preserving a similar or even better accuracy in comparison to the predictor technique. Moreover, it also seems that the EOC improves when strong coupling is employed. For more rigorous statements additional computation must be performed and analyzed. Since the computation of the corrector is usually very cheap (a very good initial guess of the solution from the

previous iteration is available), it is recommended to use the strong coupling technique whenever it is possible.

Rate of convergence	Technique	
variable	Predictor	Predictor-Corrector
h	0.8915	1.3226
τ	1.5588	2.0138

TABLE 6.3
Mean average EOC of the predictor and the predictor-corrector technique.

7. Conclusion. We developed a numerical method and a program code for solving interaction between the two-dimensional viscous incompressible fluid flow in time-dependent domains and elastic walls. We focused on a single elastic wall located on the lower side of the channel. A modification which would account for a couple of elastic walls is fairly straight-forward. The resulting algorithm was programmed in the C language. The obtained results suggest that the developed numerical scheme for the solution to the problem of interaction is sufficiently robust and it is possible to extend its scope of application by further development.

In the future work the authors would like to extend the presented model to a more complicated problem of the interaction between incompressible or compressible flow and an elastic vibrating two-dimensional body with two degrees of freedom. The model will then be applied to computing airflow around a vibrating airfoil, which can be deformed, move in the vertical direction and rotate around its elastic axis.

REFERENCES

[1] F. BREZZI AND R. S. FALK, *Stability of higher-order Hood-Taylor methods*, SIAM J. Numer. Anal., no. 28 (1991), pp. 581–590.
[2] T. A. DAVIS AND I. S. DUFF, *An unsymmetric-pattern multifrontal method for sparse LU factorization*, SIAM Journal on Matrix Analysis and Applications, vol 18, no. 1 (1997), pp. 140–158.
[3] M. FEISTAUER, *Mathematical Methods in Fluid Dynamics*, Longman Scientific & Technical, Harlow, 1993.
[4] M. A. FERNÁNDEZ AND J.-F. GERBEAU, *Algorithms for fluid-structure interaction problems*, In: L. Formaggia, A. Quarteroni and A. Veneziani, eds., Cardiovascular mathematics. Modeling and simulation of the circulatory system, Springer-Verlag Italia (2009), Springer Verlag, pp. 307-346.
[5] M. HADRAVA, *Numerical solution of flows in time dependent domains with elastic walls*, Master Thesis, Faculty of Mathematics and Physics, Charles University in Prague, 2010 (in Czech).
[6] A. HUNDERTMARK-ZAUŠKOVÁ AND M. LUKÁČOVÁ-MEDVIĎOVÁ, *Numerical study of shear-dependent non-Newtonian fluids in compliant vessels*, Comput. Math. Appl., Volume 60, Issue 3 (2010), pp. 572–590.
[7] F. NOBILE AND C. VERGARA, *An effective fluid-structure interaction formulation for vascular dynamics by generalized Robin conditions*, SIAM J. Sci. Comp., vol 30/2 (2008), pp. 731–763.
[8] T. NOMURA AND T. J. R. HUGHES, *An arbitrary Lagrangian-Eulerian finite element method for interaction of fluid and a rigid body*, Comp. Methods Appl. Mech. Engrg., no. 95 (1992), pp. 115–138.
[9] P. SVÁČEK, *FEMFLUID*, available online at: `http://marian.fsik.cvut.cz/~svacek/femfluid.html`, 2007.
[10] A. ZAUŠKOVÁ, *2D Navier-Stokes equations in a time dependent domain*, PhD Dissertation, Faculty of Mathematics, Physics and Informatics, Comenius Univ. Bratislava, 2006.